Biochemistry and Biophysics Reports 28 (2021) 101125

Contents lists available at ScienceDirect

Biochemistry and Biophysics Reports

journal homepage: www.elsevier.com/locate/bbrep

SAW1 is increasingly required to recruit Rad10 as SSA flap-length increases from 20 to 50 bases in single-strand annealing in *S. cerevisiae*

Rowen Jane Odango, Juan Camberos [1], Fred Erick Fregoso [1], Paula L. Fischhaber [*]

Department of Chemistry and Biochemistry, California State University Northridge, 18111 Nordhoff St, Northridge, CA, 91330-8262, United States

ARTICLE INFO

Keywords:
Saw1
Rad10
Double-strand break repair
Single-strand annealing

ABSTRACT

SAW1 is required by the Rad1-Rad10 nuclease for efficient removal of 3′ non-homologous DNA ends (flaps) formed as intermediates during two modes of double-strand break repair in *S. cerevisiae*, single-strand annealing (SSA) and synthesis-dependent strand annealing (SDSA). Saw1 was shown *in vitro* to exhibit increasing affinity for flap DNAs as flap lengths varied from 0 to 40 deoxynucleotides (nt) with almost no binding observed when flaps were shorter than 10 nt. Accordingly, our prior *in vivo* fluorescence microscopy investigation showed that *SAW1* was not required for recruitment of Rad10-YFP to DNA double-strand breaks (DSBs) when flaps were ~10 nt, but it was required when flaps were ~500 nt in G1 phase of the cell cycle. We were curious whether we would also observe an increased requirement of *SAW1* for Rad10 recruitment *in vivo* as flaps varied from ~20 to 50 nt, as was shown *in vitro*. In this investigation, we utilized SSA substrates that generate 20, 30, and 50 nt flaps *in vivo* in fluorescence microscopy assays and determined that *SAW1* becomes increasingly necessary for SSA starting at about ~20 nt and is completely required at ~50 nt. Quantitative PCR experiments corroborate these results by demonstrating that repair product formation decreases in the absence of *SAW1* as flap length increases. Experiments with strains containing fluorescently labeled Saw1 (Saw1-CFP) show that Saw1 localizes with Rad10 at SSA foci and that about half of the foci containing Rad10 at DSBs do not contain Saw1. Colocalization patterns of Saw1-CFP are consistent regardless of the flap length of the substrate and are roughly similar in all phases of the cell cycle. Together, these data show that Saw1 becomes increasingly important for Rad1-Rad10 recruitment and SSA repair in the ~20–50 nt flap range, and Saw1 is present at repair sites even when not required and may depart the repair site ahead of Rad1-Rad10.

1. Introduction

1.1. Steps of DSB repair and role of Rad1-Rad10

DSB repair pathways contain many genes with overlapping functions in multiple subpathways [1]. This complexity is necessary to enable repair in all phases of the cell cycle and in numerous contexts [2]. When DSBs form between DNA repeats, for example, single-strand annealing (SSA) is usually the pathway utilized in *S. cerevisiae* even though it results in the elimination of DNA lying between the repeats [1,3]. In SSA, DSB ends located between repeats are resected in a 5′→3′ fashion generating 3′ single-stranded ends that become annealed by Rad52 in a process that is generally *RAD51*-independent [4]. The DNA sequence originally situated between the repeats becomes two overhanging 3′-flaps that are hydrolyzed by the Rad1-Rad10 nuclease before ligation, eliminating the flap sequences and one repeat [5]. In higher eukaryotes, many diseases are associated with DNA repeat instability, including breast cancer and leukemia [6,7].

1.2. Saw1 and role of flap-length in Rad1-Rad10 recruitment

In *S. cerevisiae*, SSA requires *SAW1* and mutation of *SAW1* is epistatic to *rad1Δ*, *slx4Δ*, *msh2Δ*, and *rad52Δ* [8]. Chromatin immunoprecipitation experiments showed that *SAW1* is needed in order to recruit Rad1 to

Abbreviations: DIC, differential interference contrast; DSBs, double-strand breaks; nt, deoxynucleotide; SC, synthetic complete; SDSA, synthesis-dependent strand annealing; SSA, single-strand annealing; tetO, tetracycline operator; TetR, tetracycline repressor; WT, wild-type.

* Corresponding author. Department of Chemistry & Biochemistry, California State University Northridge, College of Science and Mathematics, 18111 Nordhoff ST, Northridge, CA, 91330-8262, United States.

E-mail address: paula.fischhaber@csun.edu (P.L. Fischhaber).

[1] These authors contributed equally to the work.

https://doi.org/10.1016/j.bbrep.2021.101125

Received 9 July 2021; Received in revised form 27 August 2021; Accepted 30 August 2021

Table 1
Strains used.

Name	Descriptor (for strains used in these experiments)	Genotype	Where obtained/ published
W303-1A		*MAT***a** *ade2-1 lys2Δ trp1-1 can1-100 his 3-11,15 leu2-3112 ura3-1 rad5-535*	[20]
PF025-7A		*MAT***a** *ade2-1 LYS2 trp1-1 can1-100 his 3-11,15 leu2-3112 ura3-1 TetR-mRFP (iYGL119W) URA3::tetOx224 (iYER187W) I-SceI (iYER186C) RAD10-YFP*	[16]
PF129-12A		*MAT***α** *ADE2 lys2Δ trp1-1 can1-100 his 3-11,15 leu2-3112 ura3-1 RAD10-YFP rad1::LEU2*	This manuscript
PF161–26B		*MAT***α** *ade2-1 lys2Δ trp1-1 can1-100 his 3-11,15 leu2-3112 ura3-1 TetR-mRFP (iYGL119W) URA3:: tetOx224(iYER187W) HIS3::I-SceI::HIS3 (iYER186C) RAD10-YFP saw1::LEU2*	[13]
PF180–11B		*MAT***α** *ade2-1 LYS2 trp1-1 can1-100 his 3-11,15 leu2-3112 ura3-1 TetR-mRFP (iYGL119W) URA3::tetOx224 (iYER187W) HIS3::I-SceI::HIS3 (iYER186C) RAD10-YFP rad51::LEU2*	This manuscript
PF190-17D		*MAT***α** *ade2-1 LYS2 trp1-1 can1-100 his 3-11,15 leu2-3112 ura3-1 TetR-mRFP (iYGL119W) URA3::tetOx224 (iYER187W) HIS3::500bp:I-SceI:500bp::HIS3 (iYER186C) RAD10-YFP rad52::LEU2*	[13]
PF229		*MAT***α** *ADE2 lys2Δ TRP1 can1-100 his 3-11,15 leu2-3112 ura3-1 bar1::LEU2 SAW1-CFP*	This manuscript
PF245		*MAT***a** *ade2-1 LYS2 trp1-1 can1-100 his 3-11,15 leu2-3112 ura3-1 TetR-mRFP (iYGL119W) URA3::tetOx224 (iYER187W) HIS3:10bp:I-SceI:10bp:HIS3 (iYER186C) RAD10-YFP*	This manuscript
PF246		*MAT***a** *ade2-1 LYS2 trp1-1 can1-100 his 3-11,15 leu2-3112 ura3-1 TetR-mRFP (iYGL119W) URA3::tetOx224 (iYER187W) HIS3:40bp:I-SceI:40bp:HIS3 (iYER186C) RAD10-YFP*	This manuscript
PF265–24B	20 nt Saw1-CFP	*MAT***a** *ade2-1 LYS2 trp1-1 can1-100 his 3-11,15 leu2-3112 ura3-1 TetR-mRFP (iYGL119W) URA3::tetOx224 (iYER187W) HIS3:10bp:I-SceI:10bp:HIS3 (iYER186C) RAD10-YFP SAW1-CFP*	This manuscript
PF267–4C	20 nt Wild-type	*MAT***a** *ade2-1 LYS2 trp1-1 can1-100 his 3-11,15 leu2-3112 ura3-1 TetR-mRFP (iYGL119W) URA3::tetOx224 (iYER187W) HIS3:10bp:I-SceI:10bp:HIS3 (iYER186C) RAD10-YFP*	This manuscript
PF268-5D	20 nt *saw1Δ*	*MAT***a** *ade2-1 LYS2 trp1-1 can1-100 his 3-11,15 leu2-3112 ura3-1 TetR-mRFP (iYGL119W) URA3::tetOx224 (iYER187W) HIS3:10bp:I-SceI:10bp:HIS3 (iYER186C) RAD10-YFP saw1::LEU2*	This manuscript
PF269–4B	20 nt *rad51Δ*	*MAT***a** *ade2-1 LYS2 trp1-1 can1-100 his 3-11,15 leu2-3112 ura3-1 TetR-mRFP (iYGL119W) URA3::tetOx224 (iYER187W) HIS3:10bp:I-SceI:10bp:HIS3 (iYER186C) RAD10-YFP rad51::LEU2*	This manuscript
PF270–1B	20 nt *rad52Δ*	*MAT***a** *ade2-1 LYS2 trp1-1 can1-100 his 3-11,15 leu2-3112 ura3-1 TetR-mRFP (iYGL119W) URA3::tetOx224 (iYER187W) HIS3:10bp:I-SceI:10bp:HIS3 (iYER186C) RAD10-YFP rad52::LEU2*	This manuscript
PF277-141D	50 nt Saw1-CFP	*MAT***a** *ade2-1 LYS2 trp1-1 can1-100 his 3-11,15 leu2-3112 ura3-1 TetR-mRFP (iYGL119W) URA3::tetOx224 (iYER187W) HIS3:40bp:I-SceI:40bp:HIS3 (iYER186C) RAD10-YFP SAW1-CFP*	This manuscript
PF279–8B	50 nt *saw1Δ*	*MAT***a** *ade2-1 LYS2 trp1-1 can1-100 his 3-11,15 leu2-3112 ura3-1 TetR-mRFP (iYGL119W) URA3::tetOx224 (iYER187W) HIS3:40bp:I-SceI:40bp:HIS3 (iYER186C) RAD10-YFP saw1::LEU2*	This manuscript
PF280-14A	50 nt *rad51Δ*	*MAT***a** *ade2-1 LYS2 trp1-1 can1-100 his 3-11,15 leu2-3112 ura3-1 TetR-mRFP (iYGL119W) URA3::tetOx224 (iYER187W) HIS3:40bp:I-SceI:40bp:HIS3 (iYER186C) RAD10-YFP rad51::LEU2*	This manuscript
PF281-4D	50 nt *rad52Δ*	*MAT***a** *ade2-1 LYS2 trp1-1 can1-100 his 3-11,15 leu2-3112 ura3-1 TetR-mRFP (iYGL119W) URA3::tetOx224 (iYER187W) HIS3:40bp:I-SceI:40bp:HIS3 (iYER186C) RAD10-YFP rad52::LEU2*	This manuscript
PF282–9C	50 nt Wild-type	*MAT***a** *ade2-1 LYS2 trp1-1 can1-100 his 3-11,15 leu2-3112 ura3-1 TetR-mRFP (iYGL119W) URA3::tetOx224 (iYER187W) HIS3:40bp:I-SceI:40bp:HIS3 (iYER186C) RAD10-YFP*	This manuscript
PF284		*MAT***a** *ade2-1 LYS2 trp1-1 can1-100 his 3-11,15 leu2-3112 ura3-1 TetR-mRFP (iYGL119W) URA3::tetOx224 (iYER187W) HIS3:20bp:I-SceI:20bp:HIS3 (iYER186C) RAD10-YFP*	This manuscript
PF285–4C	30 nt Wild-type	*MAT***a** *ade2-1 LYS2 trp1-1 can1-100 his 3-11,15 leu2-3112 ura3-1 TetR-mRFP (iYGL119W) URA3::tetOx224 (iYER187W) HIS3:20bp:I-SceI:20bp:HIS3 (iYER186C) RAD10-YFP*	This manuscript
PF287–7B	30 nt *saw1Δ*	*MAT***a** *ade2-1 LYS2 trp1-1 can1-100 his 3-11,15 leu2-3112 ura3-1 TetR-mRFP (iYGL119W) URA3::tetOx224 (iYER187W) HIS3:20bp:I-SceI:20bp:HIS3 (iYER186C) RAD10-YFP saw1::LEU2*	This manuscript
PF288–177B	30 nt Saw1-CFP	*MAT***a** *ade2-1 LYS2 trp1-1 can1-100 his 3-11,15 leu2-3112 ura3-1 TetR-mRFP (iYGL119W) URA3::tetOx224 (iYER187W) HIS3:20bp:I-SceI:20bp:HIS3 (iYER186C) RAD10-YFP SAW1-CFP*	This manuscript
PF290–4C	30 nt *rad51Δ*	*MAT***a** *ade2-1 LYS2 trp1-1 can1-100 his 3-11,15 leu2-3112 ura3-1 TetR-mRFP (iYGL119W) URA3::tetOx224 (iYER187W) HIS3:20bp:I-SceI:20bp:HIS3 (iYER186C) RAD10-YFP rad51::LEU2*	This manuscript
PF292-3A	30 nt *rad52Δ*	*MAT***a** *ade2-1 LYS2 trp1-1 can1-100 his 3-11,15 leu2-3112 ura3-1 TetR-mRFP (iYGL119W) URA3::tetOx224 (iYER187W) HIS3:20bp:I-SceI:20bp:HIS3 (iYER186C) RAD10-YFP rad52::LEU2*	This manuscript

Strains are haploid derivatives of W303-1A and W303–1B [20], and wild-type for the *ADE2* and *RAD5* genes unless otherwise noted.

SSA sites [9]. Additionally, it was revealed that Saw1 binds flap and splayed arm DNAs, and binding of Saw1 to Rad1-Rad10 increases Rad1-Rad10 affinity for 3′-flaps [9]. Further, *SAW1* is required to recruit Rad1-Rad10 during SDSA [10].

Published work suggests Saw1 usually acts at longer flaps since *in vitro* studies showed diminished affinity of Saw1 for 3′-flaps shorter than ~30–40 nt [9]. Further, plasmid recombination assays revealed that shorter flaps exhibit a decreased requirement for both *SAW1* and *RAD1* during SSA [8,11]. In strains containing DSB substrates that generate 20 nt flaps, the *saw1Δ* mutant exhibited a slightly higher SSA efficiency than the *rad1Δ* mutant, while the results for the *saw1Δ rad1Δ* double mutant indicated that *rad1*Δ is epistatic to *saw1Δ* [8]. However, Rad1-Rad10 has long been known to bind 3′-flaps *in vitro* without Saw1 [12]. We previously showed that *SAW1* is not required for recruitment of Rad1-Rad10 to SSA sites when flaps are only ~10 nt but is required in G1 phase when flaps are ~500 nt [13]. Together, these studies showed that Saw1 mediates binding of Rad1-Rad10 to 3′-flaps, except when flaps are short, and that Rad1-Rad10 may function in some contexts without Saw1. Interestingly, our prior work revealed that despite not being required to recruit Rad1-Rad10 to SSA sites in ~10 nt flaps, Saw1 nonetheless localizes to such substrates [13].

1.3. Questions addressed in this study

Since Saw1 does not bind to flaps shorter than ~10 nt and appears to exhibit maximal binding at approximately 30–40 nt, we wanted to test whether the requirement for Saw1 in recruitment of Rad1-Rad10 to chromasomally-situated DSBs *in vivo* would also manifest in the ~20–50 nt range (the ~10 nt substrate having already been tested in our earlier work and shown not to require Saw1 [13]). We also wanted to determine if any requirement for Saw1 would extend to SSA repair, and whether Saw1 localization at repair sites would correlate with its requirement to recruit Rad1-Rad10.

2. Materials and Methods

2.1. Cloning

HIS3 (663 bp) genes were integrated so they flanked the I-*Sce*I site in YER186C in strain PF025-7A (Table 1) using adaptamer-mediated PCR

and gene transplacement [10,13]. Transformants were selected on Synthetic Complete agar lacking histidine (SC-his agar), screened by PCR, and sequenced for the *HIS3::x-bp:I-SceI:x-bp::HIS3* cassette where "x" was either 10, 20 or 40 deoxynucleotide base pairs giving rise to substrates that would contain 20, 30 or 50 deoxynucleotide flaps, respectively. The resulting strains were crossed to give rise to the strains used in microscopy and qPCR (Table 1).

2.2. Microscopy

Strains contain chromosomally integrated copies of the Tetracycline repressor protein fluorescently labeled with RFP (TetR-RFP) and 224 tandem copies of the Tetracycline operator (tetO) sequence near the I-*Sce*I restriction site at iYER186 as described [14]. This restriction site is cleaved by exogenous I-*Sce*I with 60–70% efficiency in asynchronously growing cells [14]. Strains were transformed with plasmid pWJ1320 containing the I-*Sce*I gene under a *GAL1* promoter and an *ADE2* selection marker [15]. Transformants were plated on SC–ade medium containing 2% raffinose for selection and cultured in SC–ade with raffinose liquid medium at 23 °C. Overnight cultures were diluted to 0.1 OD_{600} followed by incubation (23 °C, 3 h). DSBs were induced by adding galactose to a final concentration of 2% (w/v) and incubating the cultures (23 °C, 30 min) prior to preparation for microscopy [10].

Microscopy was carried out using a Zeiss AxioImager M1 microscope outfitted as previously described except that the Volocity Software package was version 6.3, the objective was a Plan-Apochromat 100×, 1.46 numerical aperture oil immersion lens, and the fluorescence filter sets were ET-EYFP, Chroma #49003, (λ_{ex} = 500/20, $\lambda_{dichroic}$ = 515, λ_{em} = 535/30), ET-CFP, Chroma #49001 (λ_{ex} = 436/20, $\lambda_{dichroic}$ = 455, λ_{em} = 480/40) and ET-CY3/TRITC, Chroma #49004, (λ_{ex} = 545/25, $\lambda_{dichroic}$ = 565, λ_{em} = 605/75) [16]. Integration times were 800 ms (Rad10-YFP) and 400 ms (TetR-RFP) for experiments in which only YFP and RFP were being imaged. Integration times were 400 ms (Rad10-YFP), 200 ms (Saw1-CFP) and 200 ms (TetR-RFP) for experiments in which YFP, CFP, and RFP were all being imaged. In these triple-labeled experiments, only 3 focal planes were imaged per field of cells. In all cases, focal planes were offset by 0.3 μm intervals along the Z-axis (a Z-stack). Colocalization of foci were analyzed by inspecting images from each focal plane of the Z-stack contrast enhanced as described [13]. Cells were classified as "G1", "S/G2" or "M" as previously described [13]. Unless noted, at least 100 cells were analyzed per experimental condition in each trial. Graphs report percentages calculated from sums of foci counts from three or more independent trials and were normalized to account for differences in visual acuity between researchers. Unless otherwise noted, error bars represent exact binomial confidence intervals at the 95% confidence level. Unless otherwise noted, Fisher's exact test was applied (one-tailed) to key data comparisons and significant differences are indicated ("n.s." indicates $0.05 < P$, "*" indicates $0.01 < P < 0.05$, "**" indicates $0.001 < P < 0.01$; "***" indicates $P < 0.001$). Images were prepared using Adobe Photoshop and Illustrator (Adobe Systems, Mountain View, CA).

2.3. Quantitative PCR

Strains were transformed with pWJ1320, cultured and DSB-induced as described for microscopy except that on the day of the experiment, each strain from the overnight cultures was diluted into a single 20 mL culture at an OD_{600} of 0.2. Cultures were incubated with shaking (~255 rpm, 23 °C) until the OD_{600} was 0.3 (~3 h) before inducing them. Galactose was then added to a final concentration of 2% (w/v), the culture was swirled 10 s, and then a 5.0 mL aliquot of cells was harvested as the zero-time induced sample. The remaining culture was incubated with shaking (~255 rpm, 23 °C) and 5.0 mL aliquots harvested at intermittent time intervals (0 min, 30 min, 1 h, 2 h), by centrifugation (7000 rpm, 1 min). For uninduced controls, an equivalent volume of sterile water was added instead of galactose and aliquots were collected identically to the induced samples. Immediately following the harvest of cell aliquots, genomic DNA was isolated immediately using a standard phenol:$CHCl_3$:isoamyl alcohol extraction/ethanol precipitation protocol, storing samples at −20 °C. DNA was subjected to quantitative PCR (qPCR) using Maxima SYBR Green qPCR Master Mix (2×, Thermo Scientific) on a SmartCycler II system (Cepheid) using manufacturer's instructions (version 2.0d software), but scaling reactions to 25.0 μL. A 3-step cycling protocol was used: 1 cycle (94 °C, 10 min), 45 cycles [(94 °C, 15 s), (65 °C, 25 s), (72 °C, 1 min)]. Optical reads were acquired during extension stages and product purity assayed by melt curve and agarose gel electrophoresis.

Repair products were amplified using primers 5′-d(CTGGTTAGTTAATGGGGCGGGAAGT) and 5′-d(GCAGGCAAGATAAACGAAGGCAAAG) giving a 820 bp product. Results were compared to a 1010 bp SER3 reference product amplified with primers 5′-d(TGAAGCCTTTCTCAACGGG) and 5′-d(GCACAGTGTTCTCTTGGTCG) giving a 1042 bp product. Primer efficiencies were established via standard means [17]. Averaged C_q values, error bars and statistical tests were calculated as described previously [13].

3. Results

To determine whether Saw1 is required for recruitment of the Rad1-Rad10 complex in SSA when flaps vary between 20 and 50 nt, we prepared a panel of *S. cerevisiae* strains containing an inducible DSB site installed on Chromosome V between two copies of the *HIS3* gene, so that the ~500 bp *HIS3* sequences could serve as the flanking repeats to mediate repair by SSA (Fig. 1A). These SSA substrates differ in the spacing between the *HIS3* repeats at the inducible DSB site (Fig. 1A) thereby producing flaps of different lengths and are derivatives of strains we have previously used [13]. They also contain an adjacent fluorescent label on Chromosome V comprising an array of 224 copies of the TetR binding site that bind fluorescently labeled TetR proteins expressed from another chromosome under the control of a constitutive promoter (DSB-RFP) (Fig. 1A). The strains additionally contain a fluorescently labeled Rad10 (Rad10-YFP) that allows for the detection of Rad1-Rad10 recruitment to induced DSBs (Fig. 1A). Recruitment manifests as the appearance of Rad10-YFP/DSB-RFP colocalized foci in fluorescence images (Fig. 1A lower images). Finally, strains were either wild-type in, or deleted of the *SAW1*, *RAD51* or *RAD52* genes. Following induction of DSBs and time for repair, fluorescence images were recorded and inspected for the presence of Rad10-YFP/DSB-RFP colocalized foci. Data from experiments with 20 nt strains show that Rad10-YFP/DSB-RFP foci colocalization is observed in ~19% of the cells in the wild-type strain following DSB induction while uninduced cells show ~2.0–3.0% regardless of the phase of the cell cycle (Fig. 1B). However, in the absence of the *SAW1* gene (*saw1Δ*), the percentages of cells with colocalized foci are only about 8.9–10% following induction while uninduced are similar to uninduced wild-type (Fig. 1B). This ~50% reduction was observed in both dividing and non-dividing cells and is statistically significant (Fig. 1B). These data indicate that Rad1-Rad10 recruitment to repair sites is partially dependent on *SAW1* when flaps are ~20 nt, and contrasts with our previously published ~10 nt-flap data in which there was not a statistically significant difference between wild-type and *saw1Δ* [13].

When we tested strains containing 30 or 50 nt flaps, we found an increasing reliance on *SAW1* for Rad10-YFP recruitment. Substrates with 30 nt flaps showed a ~66% reduction in induced Rad10-YFP/DSB-RFP foci in *saw1Δ* S/G2/M cells compared to wild-type S/G2/M (Figs. 1C) and 50 nt flap substrates showed no difference in foci between induced and uninduced *saw1Δ* samples in any phase of cell cycle (Fig. 1D). Interestingly, although the 30 nt flap substrate exhibited a modest 7.3% induced foci in *saw1Δ* in S/G2/M cells (vs. 1.9% in uninduced controls), *saw1Δ* G1 cells did not show any induction of foci (similar to 50 nt flap in G1), possibly indicating a subtle cell cycle dependency for *SAW1* with shorter flaps.

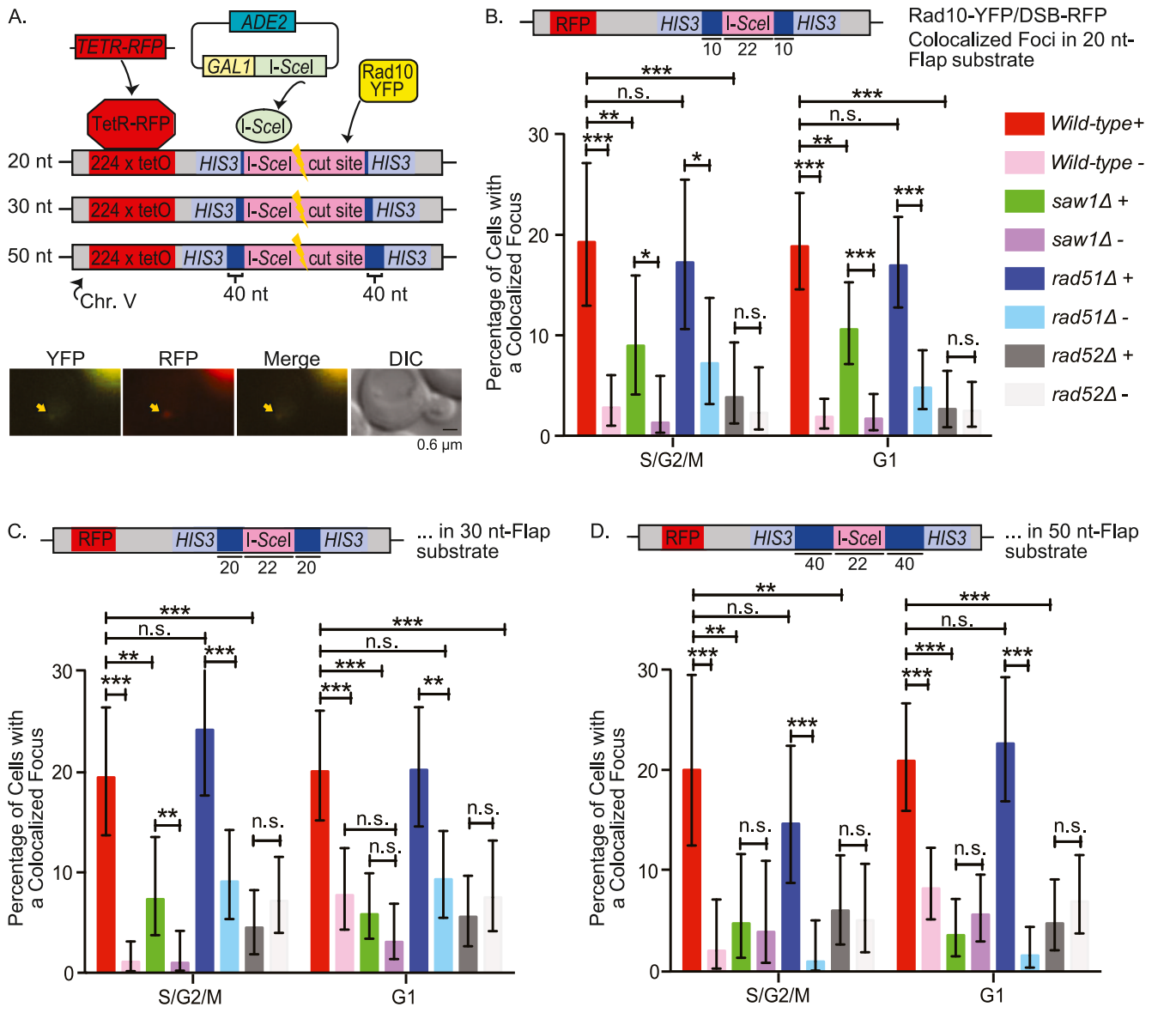

Fig. 1. Increasing requirement of *SAW1* for recruitment Rad10-YFP to SSA sites as flap length increases from 20 to 50 nt. A. Schematic showing assay system and SSA substrates. Lower panels show a cell with a colocalized focus (yellow arrow) as Rad10-YFP-only, DSB-RFP-only, Rad10-YFP/DSB-RFP merged, and DIC images. Gamma settings were adjusted slightly to make it possible to see the dim YFP focus. B-D. Cultures of yeast bearing an SSA substrate on Chromosome V and the pWJ1320 plasmid were grown to log phase, induced with galactose (+) or mock induced with water (−) and imaged. Foci in images were counted and percentages of cells containing a colocalized YFP/RFP focus were calculated and plotted as described in Materials and Methods. Graphs show results from experiments with 20 (B.), 30 (C.) or 50 (D.) nt flap-substrates. For the 50 nt substrate *saw1Δ strain*, only 291 cells total were counted for galactose-induced cells and 283 for uninduced cells (instead of ≥300). (For interpretation of the references to color in this figure legend, the reader is referred to the Web version of this article.)

We also carried out control experiments in *rad51Δ* and *rad52Δ* strain backgrounds which showed that colocalized focus induction was *RAD51*-independent but *RAD52*-dependent, indicating that repair was proceeding by SSA in all three substrates (Fig. 1B, C and 1D). Together, these data show *in vivo* that a flap size of about ~20–30 nt is the key length triggering an increasing requirement of *SAW1* for Rad1-Rad10 recruitment and that this requirement becomes absolute by ~50 nt.

We next asked whether Saw1 would localize to our SSA repair sites since, in our prior work, we observed Saw1 localizing to SSA repair sites in 10 nt as well as 500 nt flap substrates (despite *SAW1* not being required for recruitment of Rad1-Rad10 in 10 nt-flap substrates) [13]. We found ample evidence that Saw1 colocalizes at 20, 30 and 50 nt-flap substrates with Rad10-YFP; an example colocalized focus is shown (Fig. 2A). Further, results from experiments in which we quantified colocalized Rad10-YFP/Saw1-CFP/DSB-RFP foci in cells with 20, 30 and 50 nt-flap substrates were similar to each other and to the prior 10 nt-flap data (Fig. 2, B-D [13]). Specifically, we observed a significant induction of similar percentages of Rad10-YFP/Saw1-CFP/DSB-RFP foci in S/G2/M phases in all three substrates (Fig. 2B–D., 11–17%), and in G1 (Fig. 2B–D., 9–10%). Analogously to our prior report on 10 nt-flap substrates [13]. We also observed a significant induction of double foci containing only Rad10-YFP/DSB-RFP (~15% in S/G2/M, ~8–14% in G1), but very few double foci containing Saw1-CFP/DSB-RFP (~1–4% in all phases of cell cycle). These findings suggest that Saw1 and Rad1-Rad10 are recruited to the repair site at the same time, but that Saw1 may depart ahead of Rad1-Rad10 in a manner that is independent of flap length and cell cycle phase. Since Saw1-CFP is a low-abundance protein, photobleaching prevented us from imaging the entire thickness of the cells with an 11-slice Z-stack (as in Fig. 1), so these results reflect a 3-slice Z-stack. Both the presence of Saw1-CFP at all these repair sites

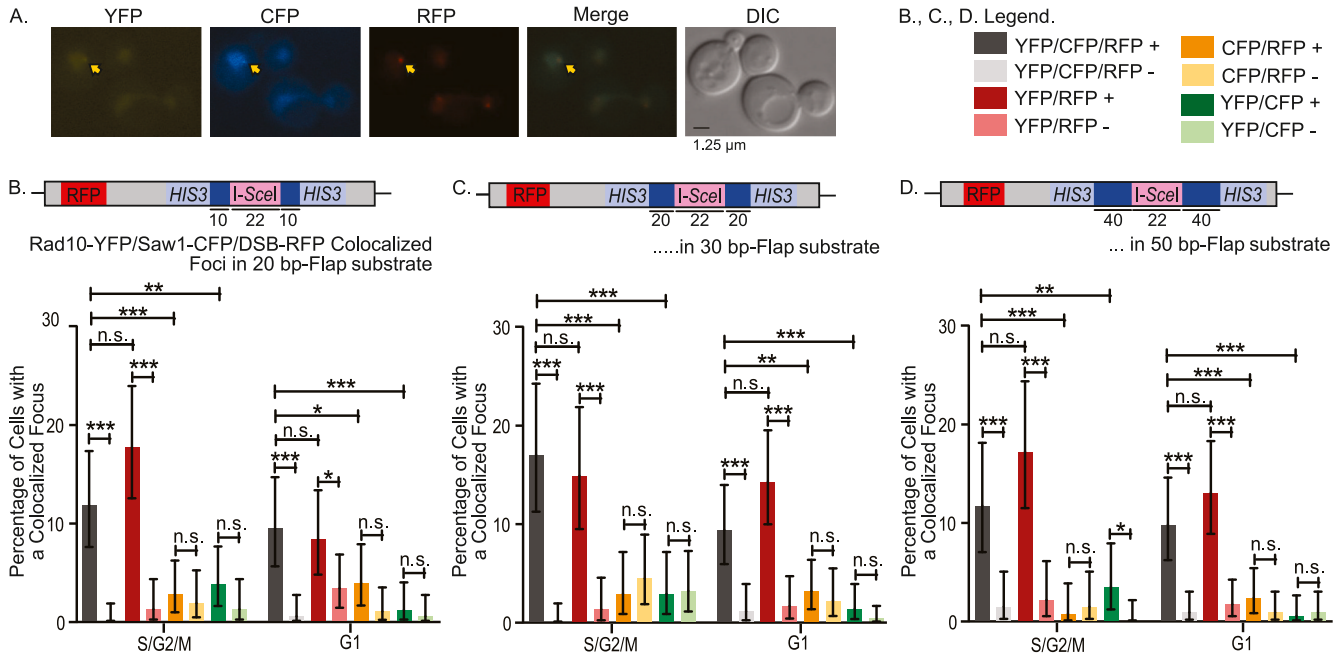

Fig. 2. Saw1 colocalizes with Rad10 at SSA sites bearing 20, 30 or 50 nt flaps. A. Fluorescence images showing a colocalized focus containing Saw1-CFP and Rad10-YFP at a DSB-RFP site. Gamma settings were adjusted slightly to see the dim CFP and YFP foci. B-D. Results from fluorescence microscopy performed analogously to Fig. 1 in which triple-labeled strains containing 20 (B.), 30 (C.) or 50 (D.) nt-flap substrates. To manage photobleaching, 3-slice Z-stacks were acquired instead of 11-slice. Foci were categorized according to the highest order focus type that applied. For example, if a focus contained all three chromophores, it counted in the YFP/CFP/RFP category only, and not in the YFP/CFP, CFP/RFP or YFP/RFP categories. Calculations and statistics were performed as described in Materials and Methods.

and the lack of flap length-dependence for this presence provide further evidence that Saw1 may be present at SSA repair sites even when it is not required for recruitment of Rad1-Rad10. We also analyzed images for the presence of Saw1-CFP/Rad10-YFP foci that were not colocalized with DSB-RFP foci and, analogously to our prior report, found that there were only background levels in all substrates (Fig. 2B–D) [13].

We next sought to establish whether we would observe repair product formation in the absence of *SAW1*. We carried out a qPCR assay in which repair product formation was monitored as a function of time in our 20, 30 and 50 nt panel of SSA strains similarly to prior work [13]. In this assay, qPCR was conducted on genomic DNA samples isolated from the same strains used in Fig. 1, following DSB induction under the same conditions. The test region amplifies the DSB site if a repair product has formed (Fig. 3A). Amplification of the test region was normalized to a control region deriving from the *SER3* gene also located on Chromosome V (Fig. 3A). Consistent with the fluorescence microscopy data in Fig. 1, we observed that there was no statistically significant difference in repair product formation between wild-type and *saw1Δ* in 20 nt strains (Fig. 3B). However, we saw significantly diminished repair product formation in 30 and 50 nt *saw1Δ* strains relative to wild-type 2 h following DSB induction, and as early as 1 h following DSB induction in 50 nt strains (Fig. 3C and D). These data corroborate our microscopy results (Fig. 1) by showing that a reduced ability to recruit Rad1-Rad10 correlates with a reduction in SSA product formation, and that the ~20–30 nt flap length triggers a dependence on Saw1 that becomes pronounced in 50 nt flap substrates. Agarose gel analysis of endpoint PCRs confirmed that the PCR products contained only the single product of the expected size (Fig. 3E).

4. Discussion

Herein, we show *in vivo* evidence that ~20–30 nt is the key flap length that triggers a requirement for *SAW1* for recruitment of the Rad1-Rad10 complex in SSA. These data expand on earlier findings that ~10 nt flaps did not require *SAW1* but that 500 nt flaps did [13]. They are also consistent with *in vitro* work showing that the binding of Saw1 to flap DNAs increases gradually as flaps vary from 10 to 50 nt [9]. A possible explanation for the necessity of Saw1 in longer flap substrates is that it aids in displacing Replication Protein A (RPA) from the single-stranded DNA region, thus making the repair site more accessible to Rad1-Rad10. To provide a visual aid, we ran Adaptive Poisson-Boltzmann Solver (APBA) Electrostatic analyses in PyMOL on the AlphaFold-predicted structure of *S. cerevisiae* Saw1, and on Rfa1 (PDB:6i52) from the scRPA trimer (Supplementary Fig.). We also included multiple sequence alignments to the closest orthologs of each (NCBI BLAST, Supplementary Fig.). The positively charged residues of the AlphaFold of Saw1 form a groove, and many of these residues are highly conserved with the closest scSaw1 orthologs (Supplemental Fig.). Interestingly, some of the charged residues in this region were previously shown to be critical for DNA binding [9]. Since scRPA binds a stretch of approximately 27–30 nt [18], a reasonable hypothesis is that the when the DNA flap is long enough to sufficiently engage RPA (~20–30 nt based on our results), Saw1 is required to dislodge RPA and help position Rad1-Rad10 at the single-strand/double-strand junction.

Interestingly, in 30 nt flaps, we detected a slight difference in the *SAW1* requirement; dividing S/G2/M cells showed a ~66% diminishment in Rad1-Rad10 recruitment to DSBs, while nondividing G1 cells showed complete loss. This indicates that Rad1-Rad10 recruitment in SSA is not mediated identically throughout the cell cycle and that *SAW1* is more important in G1. Recruitment in dividing cells may require additional proteins.

In triple-labeled experiments in which Saw1 was also fluorescently labeled, we observed Saw1 and Rad1-Rad10 frequently localized to the repair sites at the same time, in all flap substrates. Prior literature provided evidence for a Msh2-Msh3-Saw1-Rad1-Rad10 protein complex and other evidence suggesting that Msh2-Msh3 might stabilize the annealed repair intermediate thereby recruiting Saw1 and Rad1-Rad10 to the DSB site [9,19]. It is possible that Msh2-Msh3 is unable to distinguish between varying flap lengths and recruits Saw1 to all flap substrates regardless of necessity. This uniform recruitment might explain why Saw1 localizes to shorter flaps even when it is not required for Rad1-Rad10 recruitment.

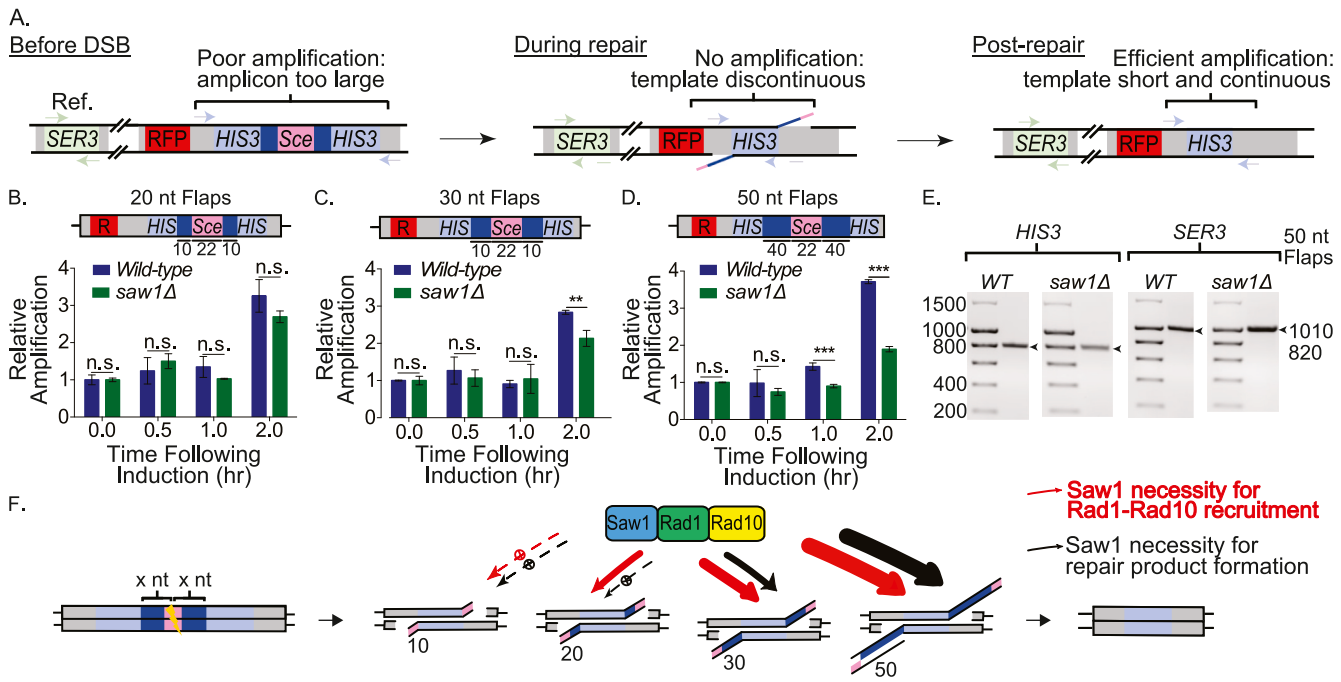

Fig. 3. Quantitative PCR shows that repair product formation is increasingly compromised in the absence of *SAW1* as flap length increases. A. Scheme illustrating qPCR strategy in which PCR amplicons were templated selectively from chromosomes having completed the ligation step of SSA. Left: prior to DSB formation (pink I-*Sce*I site) the DNA duplex is intact, but the distance between primers (periwinkle arrows flanking *HIS3* repeat cassettes) is too long to be traversed efficiently during the short extension time. Center: following DSB formation, but before ligation, the DNA duplex is not intact resulting in no amplicon formation. Right: following ligation, the distance between the primers is short and the DNA backbone intact, enabling efficient and selective product formation. *SER3* (3-phosphoglycerate dehydrogenase gene, green cassettes) is located ~30 kilobases away from the DSB site on Chromosome V and is used as the internal reference enabling normalization for template concentration. B-D. Results from qPCR experiments showing relative amplification of the SSA repair product over *SER3* reference gene normalized to the zero-time point. Calculations and statistics are described in Materials and Methods. B. 20 nt flaps, C. 30 nt flaps, and D. 50 nt flaps. E. Example agarose gel analysis of endpoint PCRs carried out as in D for the 50 nt flap substrate. F. Model for role of *SAW1* in flap-length dependent repair in SSA. The annealed intermediate formed during SSA produces flaps of a length representing the distance between each repeat and the DSB site (dark blue + pink boxes). As flap length varies from ~20 to 30 nt Saw1 is increasingly required to recruit Rad1-Rad10 to the flaps, which becomes a total requirement by ~50 nt (red arrows). This trend is also observed in formation of SSA repair products (black arrows). Increased thickness of the arrows corresponds to the increasing requirement for Saw1. (For interpretation of the references to color in this figure legend, the reader is referred to the Web version of this article.)

A significant percentage of foci were also observed that contained only Rad1-Rad10 at the repair site and not Saw1. However, there were very few foci observed that contained Saw1 at the repair site but not Rad1-Rad10, similar to our previous observations in 10 nt flap substrates [13]. Taken together these results suggest Rad1-Rad10 may be recruited to the repair site as a complex with Saw1 at all flap lengths, but that Saw1 may depart ahead of Rad1-Rad10. It is also a formal possibility that Rad1-Rad10 is sometimes recruited with Saw1 and at other times without it, but we disfavor this latter possibility since it contradicts prior data indicating that the necessity for Saw1 is flap-length dependent. Together our data support a model (Fig. 3F) in which the flap-length dependence of Saw1 for Rad1-Rad10 recruitment increases gradually over 20–30 nt, and is strongest at 50 nt.

Declaration of competing interest

The authors declare that they have no known competing financial interests or personal relationships that could have appeared to influence the work reported in this paper.

Acknowledgements

The authors thank Dr. Cristina Negritto for critical reading of the manuscript and Dr. Ravinder Abrol for guidance on the supplementary figure. This work was supported by the National Institutes of Health, grant numbers SC3GM093858 and SC1GM127204 (to P.F.), and California State University Northridge. URL: https://www.csun.edu/.

Appendix A. Supplementary data

Supplementary data to this article can be found online at https://doi.org/10.1016/j.bbrep.2021.101125.

References

[1] E.C. Friedberg, G.C. Walker, W. Siede, R.D. Wood, R.A. Schultz, T. Ellenberger, DNA Repair and Mutagenesis, 2nd. Edition, ASM Press, Washington, DC, 2005.
[2] L.S. Symington, J. Gautier, Double-strand break end resection and repair pathway choice, Annu. Rev. Genet. 45 (2011) 247–271, https://doi.org/10.1146/annurev-genet-110410-132435.
[3] E. Karathanasis, T.E. Wilson, Enhancement of Saccharomyces cerevisiae end-joining efficiency by cell growth stage but not by impairment of recombination, Genetics 161 (2002) 1015–1027.
[4] L.S. Symington, Role of RAD52 epistasis group genes in homologous recombination and double-strand break repair, Microbiology and molecular biology reviews, MMBR (Microbiol. Mol. Biol. Rev.) 66 (2002) 630–670, https://doi.org/10.1128/MMBR.66.4.630-670, table of contents.
[5] N. Sugawara, F. Paques, M. Colaiacovo, J.E. Haber, Role of Saccharomyces cerevisiae Msh2 and Msh3 repair proteins in double-strand break-induced recombination, Proc. Natl. Acad. Sci. U. S. A 94 (1997) 9214–9219, https://doi.org/10.1073/pnas.94.17.9214.
[6] Y. Miki, T. Katagiri, F. Kasumi, T. Yoshimoto, Y. Nakamura, Mutation analysis in the BRCA2 gene in primary breast cancers, Nat. Genet. 13 (1996) 245–247, https://doi.org/10.1038/ng0696-245.
[7] M.P. Strout, G. Marcucci, C.D. Bloomfield, M.A. Caligiuri, The partial tandem duplication of ALL1 (MLL) is consistently generated by Alu-mediated homologous recombination in acute myeloid leukemia, Proc. Natl. Acad. Sci. U. S. A 95 (1998) 2390–2395, https://doi.org/10.1073/pnas.95.5.2390.
[8] F. Li, J. Dong, X. Pan, J.H. Oum, J.D. Boeke, S.E. Lee, Microarray-based genetic screen defines SAW1, a gene required for Rad1/Rad10-dependent processing of recombination intermediates, Mol. Cell. 30 (2008) 325–335, https://doi.org/10.1016/j.molcel.2008.02.028.

[9] F. Li, J. Dong, R. Eichmiller, C. Holland, E. Minca, R. Prakash, P. Sung, E. Yong Shim, J.A. Surtees, S. Eun Lee, Role of Saw1 in Rad1/Rad10 complex assembly at recombination intermediates in budding yeast, EMBO J. 32 (2013) 461–472, https://doi.org/10.1038/emboj.2012.345.

[10] G. Diamante, C. Phan, A.S. Celis, J. Krueger, E.P. Kelson, P.L. Fischhaber, Saw1 is required for SDSA double-strand break repair in S. cerevisiae, Biochem. Biophys. Res. Commun. 445 (2014) 602–607, https://doi.org/10.1016/j.bbrc.2014.02.048.

[11] F. Paques, J.E. Haber, Two pathways for removal of nonhomologous DNA ends during double-strand break repair in Saccharomyces cerevisiae, Mol. Cell Biol. 17 (1997) 6765–6771.

[12] A.A. Davies, E.C. Friedberg, A.E. Tomkinson, R.D. Wood, S.C. West, Role of the Rad1 and Rad10 proteins in nucleotide excision repair and recombination, J. Biol. Chem. 270 (1995) 24638–24641, https://doi.org/10.1074/jbc.270.42.24638.

[13] M. Mardirosian, L. Nalbandyan, A.D. Miller, C. Phan, E.P. Kelson, P.L. Fischhaber, Saw1 localizes to repair sites but is not required for recruitment of Rad10 to repair intermediates bearing short non-homologous 3' flaps during single-strand annealing in S. cerevisiae, Mol. Cell. Biochem. 412 (2016) 131–139, https://doi.org/10.1007/s11010-015-2616-7.

[14] M. Lisby, U.H. Mortensen, R. Rothstein, Colocalization of multiple DNA double-strand breaks at a single Rad52 repair centre, Nat. Cell Biol. 5 (2003) 572–577, https://doi.org/10.1038/ncb997.

[15] M. Lisby, J.H. Barlow, R.C. Burgess, R. Rothstein, Choreography of the DNA damage response: spatiotemporal relationships among checkpoint and repair proteins, Cell 118 (2004) 699–713, https://doi.org/10.1016/j.cell.2004.08.015.

[16] D.M. Moore, J. Karlin, S. Gonzalez-Barrera, A. Mardiros, M. Lisby, A. Doughty, J. Gilley, R. Rothstein, E.C. Friedberg, P.L. Fischhaber, Rad10 exhibits lesion-dependent genetic requirements for recruitment to DNA double-strand breaks in Saccharomyces cerevisiae, Nucleic Acids Res. 37 (2009) 6429–6438, https://doi.org/10.1093/nar/gkp709.

[17] K.J. Livak, T.D. Schmittgen, Analysis of relative gene expression data using real-time quantitative PCR and the 2(-Delta Delta C(T)) Method, Methods 25 (2001) 402–408, https://doi.org/10.1006/meth.2001.1262.

[18] L.A. Yates, R.J. Aramayo, N. Pokhrel, C.C. Caldwell, J.A. Kaplan, R.L. Perera, M. Spies, E. Antony, X. Zhang, A structural and dynamic model for the assembly of Replication Protein A on single-stranded DNA, Nat. Commun. 9 (2018) 5447, https://doi.org/10.1038/s41467-018-07883-7.

[19] R. Eichmiller, M. Medina-Rivera, R. DeSanto, E. Minca, C. Kim, C. Holland, J. H. Seol, M. Schmit, D. Oramus, J. Smith, I.F. Gallardo, I.J. Finkelstein, S.E. Lee, J. A. Surtees, Coordination of Rad1-Rad10 interactions with Msh2-Msh3, Saw1 and RPA is essential for functional 3' non-homologous tail removal, Nucleic Acids Res. 46 (2018) 5075–5096, https://doi.org/10.1093/nar/gky254.

[20] B.J. Thomas, R. Rothstein, Elevated recombination rates in transcriptionally active DNA, Cell 56 (1989) 619–630, https://doi.org/10.1016/0092-8674(89)90584-9.